Nonlinear dynamic buckling of stiffened plates
under in-plane impact load

ZHANG Tao (张 涛)[†], LIU Tu-guang (刘土光), ZHAO Yao (赵 耀), LUO Jia-zhi (罗家智)

(*College of Traffic and Engineering, Huazhong University of Science and Technology, Wuhan 430074, China*)

[†]E-mail: icesheet@public.wh.hb.cn

Abstract: This paper presents a simple solution of the dynamic buckling of stiffened plates under in-plane impact loading. Based on large deflection theory, a discretely stiffened plate model has been used. The tangential stresses of stiffeners and in-plane displacement are neglected. Appling the Hamilton's principle, the motion equations of stiffened plates are obtained. The deflection of the plate is taken as Fourier series, and using Galerkin method the discrete equations can be deduced, which can be solved easily by Runge-Kutta method. The dynamic buckling loads of the stiffened plates are obtained form Budiansky-Roth criterion.

Key words: Stiffened plate, Dynamic buckling, In-plane impact
Document code: A   **CLC number:** O343.5

INTRODUCTION

Dynamic buckling of structures under impact loading has become a research hotspot and has received increasing attention in the last decade from designers of modern engineering structures. Most past investigations focused on simple structures such as columns, plates and cylindrical shells; papers dealing with stiffened plate structures with wide application in engineering are limited.

Zizicas (1952) investigated the dynamic buckling of thin elastic plates. A theoretical solution for simply supported rectangular plates under time-dependent in-plane loads was obtained, but neither critical condition nor buckling criterion was determined in his study. Ari-Gur *et al.*(1981) compared theoretical and experimental results of a rectangular plate impacted by a mass *M* moving in an in-plane direction, and it was clear that the dynamic buckling load of the plate is strongly de-

pendent on its initial geometric imperfection and the pulse duration. Weller *et al.*(1989) conducted studies using ADINA computer code, and calculated the dynamic load amplification factor (DLF) of metal beams and plates. They discussed mostly the influence of initial geometric imperfection and pulse duration on dynamic buckling. Petry and Fahlbush (2000) investigated the dynamic stability behavior of thin isotropic plates subjected to in-plane impact, and presented the dynamic elastic limit loads which are relatively more useful for the design of lightweight structures.

Relevant research led to the conclusion that the dynamic buckling load is strongly dependent on its initial geometric imperfection and the pulse duration based on known investigations. Previous studies indicated that investigations on the characteristics of applied loads could be divided approximately into investigations of dynamic buckling under high-velocity impact with high peak and

short duration, and investigations on low-velocity impact with low peak and long duration (Zhang *et al.*, 1993). Fluid-solid impact with wide backgrounds in military and civilian engineering is another type impact loading aside from the two impact loadings above; and is a new dynamic buckling problem of structures (Zhang *et al.*, 1992; Li *et al.*, 1993). Zhang *et al.*(1992) investigated the dynamic buckling of columns under fluid-solid impact, and carried out a large number of experimental studies. Li *et al.*(1993) experimentally investigated the plastic failure of rectangle plates under fluid-solid slamming, which is a special kind of in-plane impact loading. Cui *et al.*(1999; 2001) presented theoretical and experiment results for a plate under in-plane fluid-solid slamming. Their studies indicated that the dynamic buckling of structures under in-plane impact had dynamic response behavior; that elastic buckling was dominant for the investigated structures; and that the influences of in-plane inertia forces were not evident.

In the present work, analytical studies on the nonlinear elastic dynamic buckling of stiffened simply supported plate were conducted using a new computation method can be considered as a further development of the Galerkin method of Petry and Fahlbusch (2000). Unlike usual finite element methods, the plate and stiffeners were considered as comprising a uniform coupling system whose in-plane inertia could be neglected. Nonlinear motion equations of the stiffened plate could be obtained based on the Hamilton principle. Numerical methods can be used to get the dynamic responses of the system. The criterion of dynamic buckling loading is obtained from the Budiansky-Roth criterion (Han *et al.*, 1998). The effects of imperfections, impact duration, geometric dimension and stiffening configuration are discussed at the end of this paper.

THEORY AND ANALYSIS

Consider a stiffened rectangular thin plate under arbitrary in-plane impact loading. The dimensions and coordinate system of the structure are

shown in Fig.1. The plate is of length a and width b, and the origin denoted by O is in the middle plane of the plate. The stiffeners, modeled as beams, are placed along the plate's x-direction and y-direction respectively. The plate is subject to in-plane impact loads $p_x(t)$, $p_y(t)$ and $\tau_{xy}(t)$, and has initial imperfection w_0 in the z-direction.

(a)

(b)
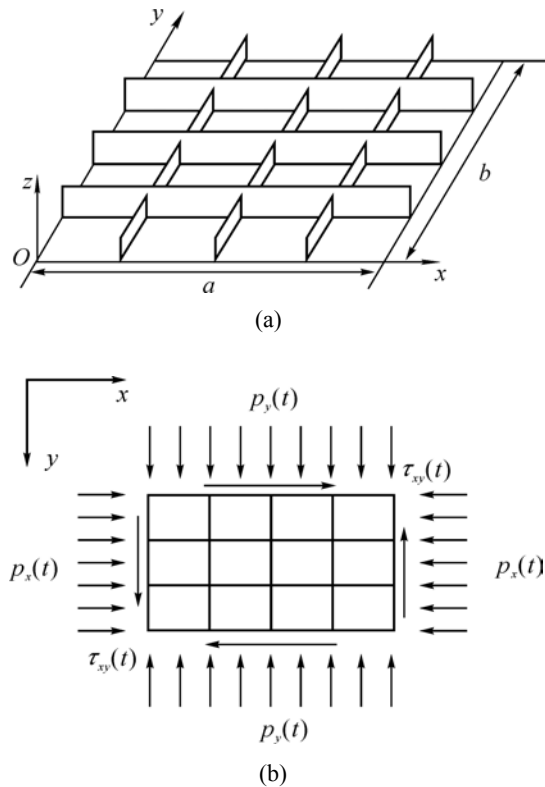
Fig.1 (a) Dimensions and coordinate system of the stiffened plate; (b) in-plane impact loadings

For the plate, effect of stress components σ_z, τ_{zx} and τ_{zy} on deformation is neglected; and for the stiffeners, torsion deformation and the effect of shear stress on deformation are also ignored. Strains of the plate section are characterized by linear Largrangian distribution; the same as of the axial strains in the stiffeners. In classic theory, the kinetic energy T and the strain energy U of the whole system could be expressed by displacements, membrane forces and bending moments; but for simplicity, the expressions are omitted here. Applying Hamilton's variation principle:

$$\delta \int_{t_2}^{t_1} (T + U + W)\mathrm{d}t = 0 .$$

where W is work done by impact load; the nonlinear motion equation of the stiffened plate may be expressed as:

$$N_x \frac{\partial^2 w}{\partial x^2} + N_y \frac{\partial^2 w}{\partial y^2} + 2N_{xy} \frac{\partial^2 w}{\partial x \partial y} + \sum_{i=1}^{m} \left(N_{x_i} \frac{\partial^2 w}{\partial x^2} \right.$$
$$\left. + \frac{\partial^2 M_{x_i}}{\partial x^2} \right) \delta_{y_i} + \sum_{j=1}^{n} \left(N_{y_j} \frac{\partial^2 w}{\partial y^2} + \frac{\partial^2 M_{y_j}}{\partial y^2} \right) \delta_{x_j}$$
$$- D(\Delta\Delta w - \Delta\Delta w_0)$$
$$= \rho h \frac{\partial^2 w}{\partial t^2} + \sum_{i=1}^{m} \rho_i h_i \frac{\partial^2 w}{\partial t^2} \delta_{y_i} + \sum_{j=1}^{n} \rho_j h_j \frac{\partial^2 w}{\partial t^2} \delta_{x_j} \qquad (1)$$

where the complex processes of the mathematical transform are omitted also for simplicity, and the in-plane and rotary inertia of the structure are neglected as previously discussed. The subscript i and j denote respectively the sequence number of the stiffeners modeled as beams along the x-direction and y-direction. In this paper all the parameter of stiffeners can be identified by their subscripts. D is the plate stiffness; Δ is the Laplacian operator; w is total transverse displacement of the plate; h is thickness of the plate; and ρ, ρ_i, and ρ_j are mass per unit volume of plate and stiffeners respectively.

Where δ_{x_j} and δ_{y_i} delta functions defined as:

$$\delta(x - x_j) = \begin{cases} 1 & (x \in [x_j - t_j / 2, x_j + t_j / 2]) \\ 0 & \text{otherwise} \end{cases};$$
$$\delta(y - y_i) = \begin{cases} 1 & (y \in [y_i - t_i / 2, y_i + t_i / 2]) \\ 0 & \text{otherwise} \end{cases}$$

t_i, y_i and t_j, x_j are the width and position of the ith stiffener along x-direction and the jth stiffener along y-direction respectively. The definition of membrane forces presumes that the shear stresses of the stiffeners can be neglected. We introduce Airy's stress function of the plate φ which satisfies

$$N_x = h \frac{\partial^2 \varphi}{\partial y^2}, N_y = h \frac{\partial^2 \varphi}{\partial x^2} \text{ and } N_{xy} = -h \frac{\partial^2 \varphi}{\partial x \partial y}, \qquad (2)$$

Bending moments of the plate may be expressed by deflection w according to large deflection theory. The axial strains of the stiffeners ε_{x_i}, ε_{y_j} are taken to be

$$\begin{cases} \varepsilon_{x_i} = \varepsilon_x^{\mathrm{o}} - z \dfrac{\partial^2 w}{\partial x^2} & (\dfrac{h}{2} \leq z \leq \dfrac{h}{2} + h_i) \\[3mm] \varepsilon_{y_j} = \varepsilon_y^{\mathrm{o}} - z \dfrac{\partial^2 w}{\partial y^2} & (\dfrac{h}{2} \leq z \leq \dfrac{h}{2} + h_j) \end{cases}$$

where superscript 'o' denotes middle-plane strains of the plate. The axial membrane forces M_{x_i}, M_{y_j} and bending moments M_{x_i}, M_{y_j} of the stiffeners can be expressed by the deflection w and the middle-plane strains of the plate and are related to the membrane forces of the plate only, so that the axial membrane forces of the stiffeners can be derived as:

$$\begin{cases} N_{x_i} = \dfrac{E_i h_i}{E} \left(\dfrac{\partial^2 \varphi}{\partial y^2} - v \dfrac{\partial^2 \varphi}{\partial x^2} \right) \delta_{y_i} - E_i e_i h_i \dfrac{\partial^2 w}{\partial x^2} \delta_{y_i} \\[3mm] N_{y_j} = \dfrac{E_j h_j}{E} \left(\dfrac{\partial^2 \varphi}{\partial x^2} - v \dfrac{\partial^2 \varphi}{\partial y^2} \right) \delta_{x_j} - E_j e_j h_j \dfrac{\partial^2 w}{\partial y^2} \delta_{x_j} \end{cases} \quad (3)$$

The bending moments of the stiffeners also may be expressed by stress function φ and deflection w

$$\begin{cases} M_{x_i} = \dfrac{E_i e_i h_i}{E} \left(\dfrac{\partial^2 \varphi}{\partial y^2} - v \dfrac{\partial^2 \varphi}{\partial x^2} \right) \delta_{y_i} - E_i I_{x_i} \dfrac{\partial^2 w}{\partial x^2} \delta_{y_i} \\[3mm] M_{y_j} = \dfrac{E_j e_j h_j}{E} \left(\dfrac{\partial^2 \varphi}{\partial x^2} - v \dfrac{\partial^2 \varphi}{\partial y^2} \right) \delta_{x_j} - E_j I_{y_j} \dfrac{\partial^2 w}{\partial y^2} \delta_{x_j} \end{cases} \quad (4)$$

where $E_i I_{x_i}$ and $E_j I_{y_j}$ are the flexural rigidities of the stiffeners, h_i and h_j are the heights of the stiffeners in x-direction and y-direction respectively. Eccentricities of the stiffeners are $e_i = (h_i + h)/2$, $e_j = (h_j + h)/2$. Substituting Eqs.(2)−(4) into Eq.(1), and applying non-dimensional transform, the motion equation of the stiffened plate could be obtained as:

$$\lambda^2 \left(\frac{\partial^2 \tilde{\varphi}}{\partial \zeta^2} \frac{\partial^2 \tilde{w}}{\partial \eta^2} + \frac{\partial^2 \tilde{\varphi}}{\partial \eta^2} \frac{\partial^2 \tilde{w}}{\partial \zeta^2} - 2 \frac{\partial^2 \tilde{\varphi}}{\partial \zeta \partial \eta} \frac{\partial^2 \tilde{w}}{\partial \zeta \partial \eta} \right)$$

$$+ \sum_{i=1}^{m} \left(C_1^i \lambda^2 \frac{\partial^2 \tilde{\varphi}}{\partial \eta^2} \frac{\partial^2 \tilde{w}}{\partial \zeta^2} - \nu C_1^i \frac{\partial^2 \tilde{\varphi}}{\partial \zeta^2} \frac{\partial^2 \tilde{w}}{\partial \zeta^2} + \lambda^2 C_2^i \frac{\partial^4 \tilde{\varphi}}{\partial \zeta^2 \partial \eta^2} \right.$$

$$\left. - \nu C_2^i \frac{\partial^4 \tilde{\varphi}}{\partial \zeta^4} \right) \delta_{y_i} + \sum_{j=1}^{n} \left(\lambda^2 C_1^j \frac{\partial^2 \tilde{\varphi}}{\partial \zeta^2} \frac{\partial^2 \tilde{w}}{\partial \eta^2} - \nu \lambda^4 C_1^j \frac{\partial^2 \tilde{\varphi}}{\partial \eta^2} \frac{\partial^2 \tilde{w}}{\partial \eta^2} \right.$$

$$\left. + \lambda^2 C_2^j \frac{\partial^4 \tilde{\varphi}}{\partial \zeta^2 \partial \eta^2} - \nu \lambda^4 C_2^j \frac{\partial^4 \tilde{\varphi}}{\partial \eta^4} \right) \delta_{x_j}$$

$$= \frac{1}{12(1-\nu^2)} \left[\left(\frac{\partial^4 \tilde{w}}{\partial \zeta^4} + 2\lambda^2 \frac{\partial^4 \tilde{w}}{\partial \zeta^2 \partial \eta^2} + \lambda^4 \frac{\partial^4 \tilde{w}}{\partial \eta^4} \right) \right.$$

$$\left. - \left(\frac{\partial^4 \tilde{w}_0}{\partial \zeta^4} + 2\lambda^2 \frac{\partial^4 \tilde{w}_0}{\partial \zeta^2 \partial \eta^2} + \lambda^4 \frac{\partial^4 \tilde{w}_0}{\partial \eta^4} \right) \right]$$

$$+ \sum_{i=1}^{m} \left(C_2^i \frac{\partial^2 \tilde{w}}{\partial \zeta^2} \frac{\partial^2 \tilde{w}}{\partial \zeta^2} + C_3^i \frac{\partial^4 w}{\partial \zeta^4} \right) \delta_{y_i} + \sum_{j=1}^{n} \lambda^4 \left(C_2^j \frac{\partial^2 \tilde{w}}{\partial \eta^2} \frac{\partial^2 \tilde{w}}{\partial \eta^2} \right.$$

$$\left. + C_3^j \frac{\partial^4 \tilde{w}}{\partial \eta^4} \delta_{x_j} \right) + \lambda^4 \frac{\partial^2 \tilde{w}}{\partial \tau^2} + \sum_{i=1}^{m} \lambda^4 C_4^i \frac{\partial^2 \tilde{w}}{\partial \tau^2} \delta_{y_i}$$

$$+ \sum_{i=1}^{m} \lambda^4 C_4^j \frac{\partial^2 \tilde{w}}{\partial \tau^2} \delta_{x_j} \tag{5}$$

where ν is Poisson's ratio. The other non-dimensional parameters and constants are defined in the Appendix. According to Marguerre's theory (Eivind, 1989), the compatibility equation of the plate is

$$\left(\lambda^4 \frac{\partial^4 \tilde{\varphi}}{\partial \eta^4} + 2\lambda^2 \frac{\partial^4 \tilde{\varphi}}{\partial \zeta^2 \partial \eta^2} + \frac{\partial^4 \tilde{\varphi}}{\partial \zeta^4} \right)$$

$$= \lambda^2 \left[\left(\frac{\partial^2 \tilde{w}}{\partial \zeta \partial \eta} \right)^2 - \frac{\partial^2 \tilde{w}}{\partial \zeta^2} \frac{\partial^2 \tilde{w}}{\partial \eta^2} - \left(\frac{\partial^2 \tilde{w}_0}{\partial \zeta \partial \eta} \right)^2 + \frac{\partial^2 \tilde{w}_0}{\partial \zeta^2} \frac{\partial^2 \tilde{w}_0}{\partial \eta^2} \right] \tag{6}$$

In accordance with the boundary conditions for the simply supported plate, Navier's double Fourier series with coefficients f_{pq}^{τ} and f_{pq}^{0} are chosen to describe the non-dimension displacement function $\tilde{w}$ and the initial geometric imperfection $\tilde{w}_0$:

$$\begin{cases} \tilde{w}_0 = \sum_{p=1}^{I} \sum_{q=1}^{J} f_{pq}^{o} \sin p\pi\zeta \sin q\pi\eta \\ \tilde{w} = \sum_{p=1}^{I} \sum_{q=1}^{J} f_{pq}^{\tau} \sin p\pi\zeta \sin q\pi\eta \end{cases} \tag{7}$$

where superscript 'o' denotes $\tau=0$, superscript 'τ' denotes the function with parameter τ. And $\tilde{w}(\tau = 0) = \tilde{w}_0$. Substituting Eq.(7) into Eq.(6), and using trigonometric relations, Airy's stress function $\tilde{\varphi}$ can be derived as:

$$\tilde{\varphi} = \frac{1}{2} \bar{N}_\zeta \eta^2 + \frac{1}{2} \bar{N}_\eta \zeta^2 - \bar{N}_{xy} \zeta\eta + \sum_{p=1}^{\infty} \sum_{q=1}^{\infty} \left(A_1^{pq} \cos 2p\pi\zeta \right.$$

$$\left. + A_2^{pq} \cos 2q\pi\eta \right) \cdot \left(f_{pq}^{\tau\,2} - f_{pq}^{o\,2} \right) + \sum_{p=1}^{\infty} \sum_{q=1}^{\infty} \sum_{l=1}^{\infty} \sum_{k=1}^{\infty} {}^{(p,q)\neq(l,k)} \left\{ A_3^{pqlk} \cdot \right.$$

$$\cos(p-l)\pi\zeta \cos(q-k)\pi\eta + A_4^{pqlk} \cos(p-l)\pi\zeta \cdot$$

$$\cos(q+k)\pi\eta + A_5^{pqlk} \cos(p+l)\pi\zeta \cos(q-k)\pi\eta$$

$$\left. + A_6^{pqlk} \cos(p+l)\pi\zeta \cos(q+k)\pi\eta \right\} \cdot \left(f_{pq}^{\tau} f_{lk}^{\tau} - f_{pq}^{o} f_{lk}^{o} \right) \tag{8}$$

The meaning of A_i^{pqlk} is defined in Appendix. The constants $\bar{N}_\zeta, \bar{N}_\eta$ and $\bar{N}_{\zeta\eta}$ may be defined by the boundary conditions as follows:

$$x = 0, a: \frac{Eh^2}{b^2} \int_0^1 \frac{\partial^2 \tilde{\varphi}}{\partial \eta^2} \mathrm{d}\eta = P_x; -\frac{Eh^2}{b^2} \int_0^1 \frac{\partial^2 \tilde{\varphi}}{\partial \zeta \partial \eta} \mathrm{d}\eta = \tau_{xy};$$

$$y = 0, b: \frac{Eh^2}{a^2} \int_0^1 \frac{\partial^2 \tilde{\varphi}}{\partial \zeta^2} \mathrm{d}\zeta = P_y; -\frac{Eh^2}{a^2} \int_0^1 \frac{\partial^2 \tilde{\varphi}}{\partial \zeta \partial \eta} \mathrm{d}\zeta = \tau_{xy};$$

P_x, P_y and τ_{xy} are non-dimensional in-plane fluid-solid impact load, and can be defined by the impact function with two parameters as follows (Zhang et al., 1992):

$$p(t) = \begin{cases} \eta_1 t^2 + \eta_2 t & (0 \le t \le T_d) \\ 0 & (t > T_d) \end{cases}$$

where $\eta_1 = -4P_{max}/T_d^2$, $\eta_2 = 4P_{max}/T_d$, P_{max} is the peak value and T_d is the duration of the impact loading.

Inserting Airy's stress function defined by Eq.(8) satisfying relevant boundary conditions into the nonlinear equation of Eq.(5), multiplying by $\sin r\pi\zeta \sin s\pi\eta$ ($r=1, 2, \cdots, R$; $s=1, 2, \cdots, S$) and integrating over the plate area yields a set of second-order ordinary differential equations for computing

the coefficients f_{rs}^{τ} of the double Fourier series:

$$\sum_{r=1}^{R}\sum_{s=1}^{S}M_{ijrs}\ddot{f}_{rs}^{\tau}+\sum_{r=1}^{R}\sum_{s=1}^{S}K_{ijrs}(f_{rs}^{\tau}-f_{rs}^{o})$$
$$+\sum_{r=1}^{R}\sum_{s=1}^{S}\sum_{l=1}^{R}\sum_{k=1}^{S}D_{ijrslk}(f_{rs}^{\tau}f_{lk}^{\tau}-f_{rs}^{o}f_{lk}^{o}) \qquad (9)$$
$$+\sum_{r=1}^{R}\sum_{s=1}^{S}\sum_{l=1}^{R}\sum_{k=1}^{S}\sum_{p=1}^{R}\sum_{q=1}^{S}F_{ijrslkpq}(f_{rs}^{\tau}f_{lk}^{\tau}-f_{rs}^{o}f_{lk}^{o})f_{pq}^{\tau}$$
$$=0 \qquad (i=1,2,3\cdots R;\ j=1,2,3\cdots S)$$

where expressions of the coefficients M_{ijrs}, K_{ijrs}, D_{ijrs}, F_{ijrs} are too complex to be defined in the formulas although their values can be obtained by computation. The dynamic responses of the stiffened plate system can be obtained from the results of Eq.(9); whose initial conditions are $f_{rs}^{\tau}(\tau=0)$ $=f_{rs}^{o}$, $\dot{f}_{rs}^{\tau}(\tau=0)=0$. A fourth-order Runge-Kutta method for time integration was used to solve the equations. Increase of R and S increases the CPU time nearly cubically and the equations may be become unmanageable. In the fact, only 9 terms of Fourier series are taken in the calculation. This is satisfactory for getting a good resolution.

Under in-plane fluid-solid impact, the buckling of the stiffened plates is dynamic response type buckling, and has stable post-buckling path state. The Budiansky-Roth criterion may be used to estimate the dynamic buckling. With increase of impact time, the initial geometrical imperfection of the structure increases too; when the increase of the imperfection becomes sharp suddenly, we can infer that dynamic buckling of the structure has occurred.

RRESULTS AND DISCUSSION

Plate without stiffeners

In view of the limited on dynamic buckling of stiffened plate, example results are presented for a plate without stiffeners and compared with the Weller *et al.*(1989)'s results in order to validate the theory and analysis of the present paper.

The plate specimen used for calculation in the present paper had the following parameters: length

a=150 mm; width b=150 mm; thickness h=1.6 mm; Young's modulus E=7.06×10^4 N/mm^2; density ρ= 2.7×10^{-6} kg/mm^3. The plate was simply supported along all its edges, and the load was introduced through one edge. The impact loading had characteristics of a half sine wave with peak value P_x and period $T=T_b$, where T_b is the first period of lateral free vibration of the unloaded plate. The initial geometrical imperfection of the plate sinusoidal: $w_0=w_{11}\sin\pi\xi\sin\pi\eta$.

This paper's calculated results and those in the literature (Petry and Fahlbush, 2000) are shown in Fig.2 for the case when w_{11}/h=0.15625, P_x=78.4 N/mm. The solid-line curve is the deflection response of the plate center calculated by the present method; the dash-line is the result calculated with Adina programme, and the dotted-line is the result of the Implate programme. The results in this paper agreed with Petry and Fahlbusch (2000)'s results, agreed well with the results of the finite element method; were a little less than the Adina results but more than the Implate results.

The Budiansky-Roth curves of the plate center for various initial imperfections are shown in Fig.3. It was clear that with the increase of the initial imperfection w_0, the dynamic buckling of the plate occurred more easily; and that after the peak value of the impact load increased to a certain value, the responses of the plate increased sharply when w_0 was less; therefore the Budiansky-Roth criterion is fit for detecting the dynamic buckling of the plate.
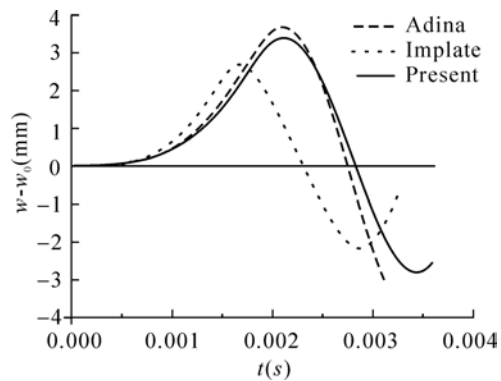
Fig.2 Time history cures of the deflection of the plate center
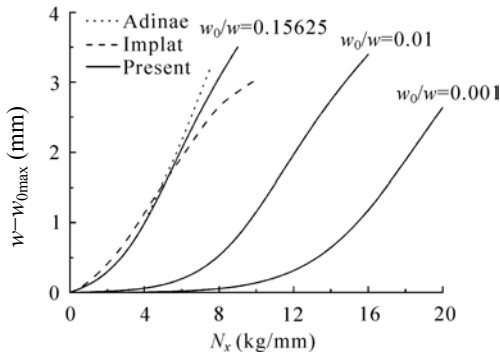
Fig.3 Plate response for various initial imperfections

However when the value of initial imperfection w_0 was rather large, there was no field with notable variety in the Budiansky-Roth curve, so it was not very suitable as a criterion. There was similar conclusion in the Wang's (1997) studies led to similar conclusion on the dynamic buckling of a column.

Stiffened plate

The geometrical dimensions and structure of the stiffened plate are shown in Fig.4. The plate with simply supported edges has one stiffener in the x-direction. The dimensions of the plate are: length a=150 mm; width b=150 mm and thickness h=1.6 mm. The stiffener has a rectangular section: $h_1 \times t_1$= 15×1.6 mm². Parameters of the plate and stiffener: Young's modulus E=7.06×10⁴ N/mm² and density ρ=2.7×10⁻⁶ kg/mm³. The in-plane impact was applied equally to the ends of the plate and stiffener in the x-direction. The peak is denoted by q and the duration was T.

1. Effects of initial imperfection

The initial imperfection had great influence on the buckling of the stiffened plates. There are three types of initial imperfection defined as: type 1: w_0= $w_{11}\sin\pi\xi\sin\pi\eta$; type 2: w_0=$w_{12}\sin\pi\xi\sin2\pi\eta$; type 3: w_0=$w_{11}\sin\pi\xi\sin\pi\eta+w_{12}\sin\pi\xi\sin2\pi\eta$. The time history curves of the deflection of the maximal response point in the plate for w_{11}=w_{12}=0.2h; q=200 N/mm² and T=T_b is shown in Fig.5, Comparison between the results of this paper and the results obtained with the Adina programme (dashed line) showed they agreed well. The solutions in the Fig.5 can be used for verification of the computational method's applicability to large deflection problem of stiffened plates (w_{max}/h>1). The buckling responses to the type 2 and type 3 to initial imperfections are close to each but much larger than the buckling response to type 1 initial imperfection; and the dynamic buckling occurs more easily. The dynamic buckling mode of the stiffened plate is shown in Fig.6, where the thick line is the stiffener. The buckling responses to two types of initial imperfection occurred in commonly observed buckling mode and were close to the first mode of lateral free vibration of the unloaded stiffened plate structure. The maximal response point was the plate center for the type 1 initial imperfection, but for the other two types it was at half of the length and a quarter of the width. In Fig.7 of the P-Y curves of the maximal response point of the stiffened plate with different initial imperfection types, P denotes the peak values of the impact loading q and Y is the response of the displacement $w-w_0$. It was concluded that when the shape of the initial imperfection

Fig.4 The structure of the stiffened plate
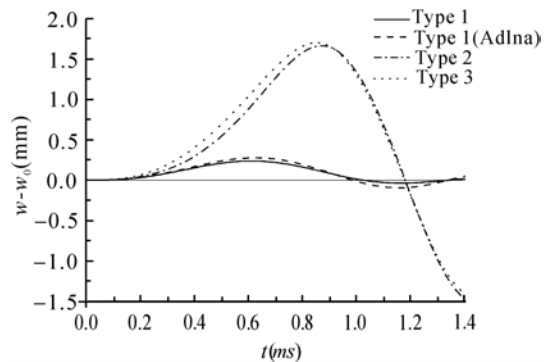
Fig.5 Time history curves of the maximal response
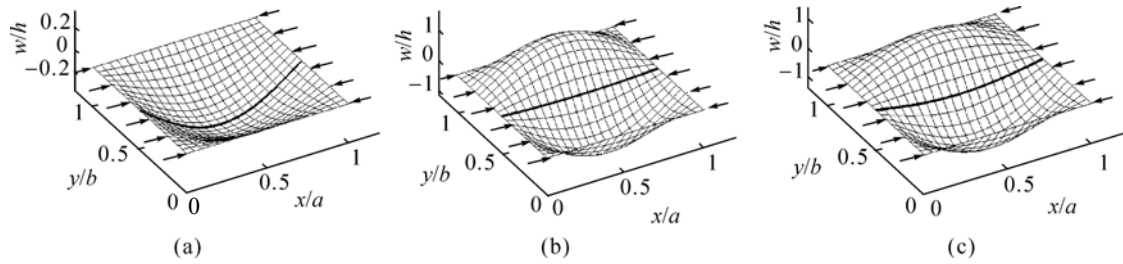
Fig.6 Buckling mode for different imperfection types
(a) Type 1; (b) Type 2; (c) Type 3
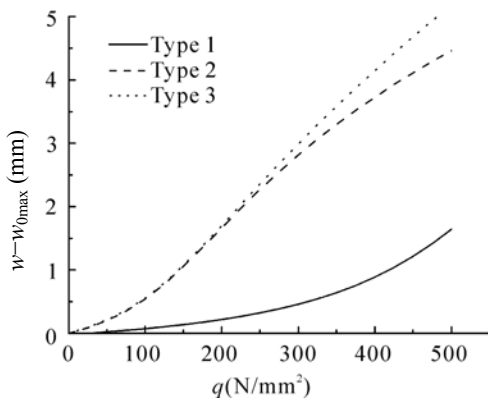
Fig.7 *P-Y* curves for different imperfection types
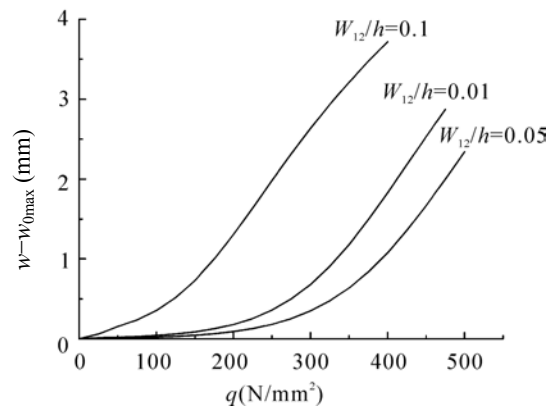
Fig.8 *P-Y* curves for different imperfection magnitudes

contains the first mode of lateral free vibration, the shape of the first mode is dominant in the dynamic buckling mode; and that the imperfection without the first mode of lateral free vibration of the structure favors the capacity to resist the impact load in the engineering design.

The imperfection sensitivity of dynamic stability behavior was pointed out in many papers (Ari-Gur *et al.*, 1981; Weller *et al.*, 1989; Petry and Fahlbusch, 2000; Zhang *et al.*, 1993). Fig.8 of the *P-Y* curves of the maximal response point for different imperfection magnitudes ($w_0 = w_{12}\sin\pi\xi\sin2\pi\eta$). As shows that higher imperfection leads to smaller buckling load.

2. Influence of the impact duration

The fluid-solid impact is a typical intermediate velocity impact whose duration is usually in the order of milliseconds, and is usually more than the duration of first period of the structure's free vibration. Elastic buckling is dominant in in-plane fluid-solid impact. The maximum of the response variation under impact peak when $T/T_b = 2$, 1, 0.5 is

shown in Fig.9. Weller *et al.*(1989) pointed out that the shorter duration of impact load, the higher is the dynamic buckling load at the same impact peak.

3. Dimensions of the stiffener

The stiffeners greatly strengthen the capacity of stiffened plate to resist buckling. For stiffener with rectangular section, the geometrical dimensions are the stiffener height h_1 and thickness t_1.
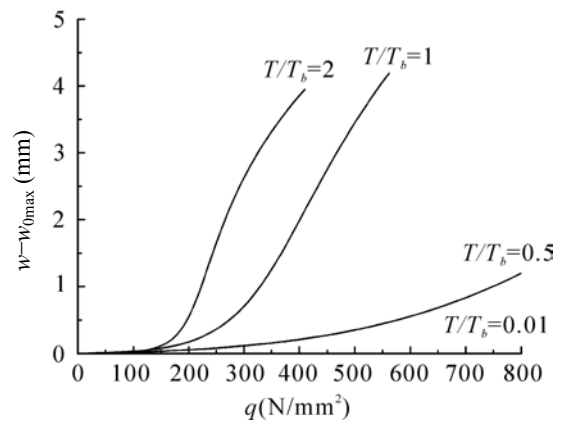
Fig.9 *P-Y* curves for different durations

The first mode of lateral free vibration is different with different dimension stiffener. As discussed before, the imperfection of the stiffened plate is described by two terms of sinusoidal waves $w_{11}\sin\pi\xi\sin\pi\eta + w_{12}\sin\pi\xi\sin2\pi\eta$. When h_1/t_1, the ratio of the stiffener height and thickness, is a constant and equal to 5, duration T=5 ms; the maximum of the response is shown in Fig.10. The buckling load increases obviously with the stiffener height; but when height reaches a certain value, the buckling load does not increase, because the local buckling of the plate that occurs is not helpful for enhancing the stiffener intensity.

4. Configuration of spacing stiffeners

An example is discussed to gain insight into the effects for various stiffening configurations. There are three stiffener spacing configurations in Fig.11. The stiffeners are evenly placed along the impact load direction, and have a fixed total weight. The dimensions of the stiffener's rectangular section are 1.6 mm

×8 mm, 1.13 mm×5.66 mm and 0.924 mm×4.62 mm respectively, where the ratio of height to thickness of each stiffener is equal to 5. Evenly dividing the total weight among several stiffeners weakens obviously the structure and reduces the buckling load.

CONCLUSION

This paper presents a dynamic buckling analysis of stiffened plates under in-plane impact load. Use of an alternative semi-numerical method in the analysis significantly economizes on CPU time and simplifies the formulations. The results of several examples were in excellent agreement with the finite element method. The analysis of results indicated that the Budiansky-Roth criterion is partially applicable for detecting the dynamic buckling of a stiffened plate. For the large imperfection, defining a critical deflection would be an alternative method. An appropriate shape of initial imperfection would avoid local buckling of the structure under impact load.
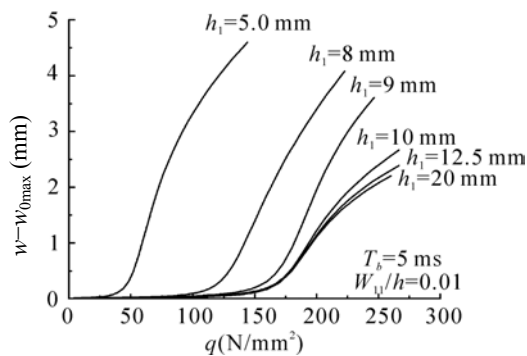
Fig.10 *P-Y* curves with different stiffener heights
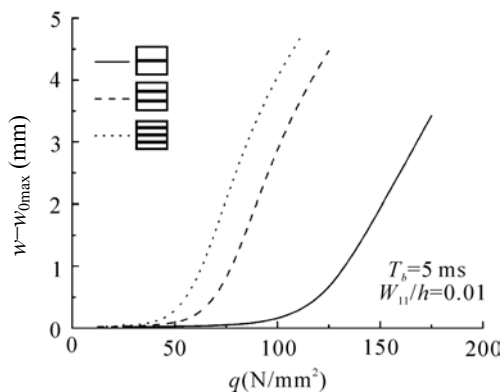
Fig.11 The *P-Y* curves with different stiffening configurations

References

Ari-Gur, J., Singer, J., Weller, T., 1981. Dynamic buckling of plates under longitudinal impact. *Israel J Techno*, **19**:57-64.

Cui, S.J., Cheong, H.K., Hao, H., 1999. Experimental study of dynamic buckling of plates under fluid-solid slamming. *Int J. Impact Engng*, (22):675-691.

Cui, S.J., Cheong, H.K., Hao, H., 2001. Numerical analysis of dynamic buckling of rectangular plates subjected to intermediate-velocity impact. *Int J. Impact Engng*, (25):147-167.

Eivind, S., 1989. Elastic buckling and postbuckling of eccentrically stiffened plates. *Int. J. Solids Structures*, **25**(7):751-768.

Han, Q., Zhang, S.Y., Yang, G.T., 1998. Advances in research for static and dynamic buckling of structure. *Advances in mechanics*, **25**(3):349-360 (in Chinese).

Li, S.Q., Zhang, Q.J., Zheng, J.J., 1993. Experimental investigation on dynamic buckling and plastic collapsing of rectangular plates subject to solid-fluid in-plane impact. *Acta Mechanica Sinica*, **25**(2):249-255 (in Chinese).

Petry, D., Fahlbusch, G., 2000. Dynamic buckling of thin isotropic plates subjected to in-plane impact. *Thin-Walled Structures*, (38):267-283.

Wang, D.Y., 1997. Axial impact buckling of a column subject to lateral static load. *Vibration & shock*, **16**(1): 35-37 (in Chinese).

Weller, T., Abramovich, H., Yaffe, R., 1989. Dynamics of beams and plates subjected to axial impact. *Comp and Struct*, **32**(3-4):835-851.

Zhang, Q.J., Li, S.Q., Zheng, J.J., 1992. Dynamic response, buckling and collapsing of elastic-plastic straight col-umns under axial solid-fluid slamming compression. *Int. J. Solids & Structures*, (29):381-397.

Zhang, Q.J., Liu, T.G., Zheng, J.J., Li, S.Q., 1993. Advances in research on dynamic buckling of structures. *Advances in mechanics*, **23**(4):530-538 (in Chinese).

Zizicas, G.A., 1952. Dynamic buckling of thin plates. *Trans ASME*, **74**(7):1257-68.

Appendix

$$C_1^i = \frac{E_i h_i}{Eh}, \ C_1^j = \frac{E_j h_j}{Eh}, \ C_2^i = \frac{E_i e_i h_i}{Eh^2}, \ C_2^j = \frac{E_j e_j h_j}{Eh^2},$$

$$C_3^i = \frac{E_i I_{x_i}}{Eh^3}, \ C_3^j = \frac{E_j I_{y_j}}{Eh^3}, \ C_4^i = \frac{h_i \rho_i}{h\rho}, \ C_4^j = \frac{h_j \rho_j}{h\rho},$$

$$\tilde{w} = \frac{w}{h}, \ \tilde{\varphi} = \frac{\varphi}{Eh^2}, \ \lambda = \frac{a}{b}, \ \zeta = \frac{x}{a}, \ \eta = \frac{y}{b}, \ \tau = \frac{t}{b^2}\sqrt{\frac{Eh^2}{\rho}} \ ,$$

$$\bar{N}_\zeta = \frac{\bar{N}_x b^2}{Eh^2}, \ \bar{N}_\eta = \frac{\bar{N}_y a^2}{Eh^2}, \ \bar{N}_{\zeta\eta} = \frac{\bar{N}_{xy} ab}{Eh^2},$$

$$A_1^{pq} = \frac{q^2}{32\lambda^2 p^2}, \ A_3^{pqlk} = \frac{(pqlk - p^2k^2)\lambda^2}{4\left[(p-l)^2 \lambda^2 + (q-k)^2\right]^2},$$

$$A_5^{pqlk} = \frac{(pqlk + p^2k^2)\lambda^2}{4\left[(p+l)^2 \lambda^2 + (q-k)^2\right]^2}, \ A_2^{pq} = \frac{\lambda^2 p^2}{32 q^2},$$

$$A_4^{pqlk} = \frac{(pqlk + p^2k^2)\lambda^2}{4\left[(p-l)^2 \lambda^2 + (q+k)^2\right]^2},$$

$$A_6^{pqlk} = \frac{(pqlk - p^2k^2)\lambda^2}{4\left[(p+l)^2 \lambda^2 + (q-k)^2\right]^2}$$